博 士 論 文

Fabrication and characterization of osteoconductive scaffold of recombinant peptide based on human collagen type I and β-tri calcium phosphate nanoparticles.
(ヒトⅠ型コラーゲン様リコンビナントペプチドと β-リン酸三カルシウムナノ粒子からなる骨形成スキャフォールドの作製および特性評価)

平成 31 年 3 月申請

北海道大学

大学院歯学研究科口腔医学専攻

降　簇　友　和

Title

Fabrication and characterization of osteoconductive scaffold of recombinant peptide based on human collagen type I and β-tri calcium phosphate nanoparticles.

Tomokazu FURIHATA, Hirofumi MIYAJI and Tsutomu SUGAYA

Institutions

Department of Periodontology and Endodontology, Hokkaido University Faculty of Dental Medicine, N13, W 7, Kita-ku, Sapporo, 060-8586, Japan.

Corresponding author

Tomokazu Furihata

E-mail: furihata@den.hokudai.ac.jp

Key words

Bone tissue engineering, rat, reverse transcription polymerase chain reaction (RT-PCR)

Running title

Bone inductive ability of RCP-TCP

Number of pages, tables and figures

25 pages, 8 figures

Abstract

Recombinant peptide based on human collagen type I has been introduced as a xeno-free polymer material for various tissue engineering approach. In this study, we fabricated the recombinant human collagen-peptide based scaffold (RCP) applied with β-TCP nanoparticles (RCP-TCP) and assessed the osteoconductive capability of RCP-TCP in cell-culture test and rat bone-forming test.

RCP-TCP was prepared by mixing the RCP granules and nanoparticulated β-TCP aqueous dispersion (0, 0.01, 0.1, 1 and 10 wt%). Subsequently, RCP-TCP was characterized using scanning electron microscopy (SEM), energy dispersive X-ray spectrometry (EDX), cyto-compatibility testing and real-time RT-PCR. In addition, RCP-TCP was implanted into the defect of rat cranial bone. Radiographic and histological evaluation was carried out at 2 and 4 weeks.

In SEM and EDX analyses, RCP-TCP showed β-TCP nanoparticles aggregated on the RCP surface and exhibited the elements of P and Ca. In cell culture tests, RCP-TCP remarkably promoted the proliferation of osteoblastic MC3T3-E1 cell and the expression of osteogenic markers, such as anti-runt-related transcription factor 2, alkaline phosphatase and bone sialoprotein resulted in osteoblastic differentiation. In the rat bone forming test, RCP-TCP significantly stimulated the new bone formation at 2 and 4 weeks,

when compared to RCP and no application groups. Therefore, RCP-TCP would be anticipated for application to bone tissue engineering therapy.

Introduction

Evolution of bone tissue engineering therapy are requested for the treatment of bone loss caused by infectious disease, trauma and cancer. It is considered that tissue engineering three elements[1]; cells[2-4], signaling molecule[5-8], and natural and artificial scaffolds[9-11] are essential for bone regenerative strategies. Scaffold plays a major role in stimulating cell proliferation and differentiation and providing growth and nutrition factors in the bone tissue defects. Polymer matrix, including collagen[12-13], hyaluronic acid[13] and poly lactic-co-glycolic acid[14], is widely known as good bioabsorbable scaffold materials. Especially, scaffold constructed with collagen had the great cellular affinity and biodegradability in regenerative therapies[15-16]. However, osteoinduction of collagen was low when compared to bioceramics[17] and the conventional collagen scaffold was delivered from xenogeneic tissues as bovine and pig[18]. Hence, these disadvantages of collagen substrate need to be solved by novel concept to develop novel collagen scaffold.

Bio-safe bioceramics, including beta-tricalcium phosphate (β-TCP), hydroxyapatite, octacalcium phosphate[19], bioactive glass and composites, have been clinically applied to bone graft materials[20-21]. Bioceramics material possessed high strength and continuous CaP supplying to obtain the bone inductive ability, however, low bioabsorbable ability to be long-term residue in the body[22]. Recently, nano-structured

bioceramics were introduced into regenerative approach of bone tissue engineering because of its great degradability. In addition, nanoparticulated bioceramics exhibited the bioactive effects to stimulate wound healing and regeneration, as well as biodegradation. Joseph et al. demonstrated that nanostructured apatite layer created onto the collagen scaffold remarkably promoted the cellular response, such as blood vessels ingrowth and macrophage accumulation, into the scaffold[23]. Furthermore, Murakami et al. created the collagen scaffold applied with β-TCP nanoparticles. The scaffold stimulated not only bone induction but biodegradation when compared to normal type[17]. Hence, improvements of collagen scaffold via nano-bioceramic application may play a major role in up-regulation of the quality and quantity of newly engineered bone.

Recently, gene recombination technology solved the problem of xenogeneic material. Pawelec et al. had the first presentation about the biocompatibility of the recombinant human collagen-peptide based scaffold (RCP). The peptide was enriched with arginyl-glycyl-aspartic acid (RGD) groups to contribute the cell adhesion, cellular spreading and differentiation[24]. In addition, some investigators reported the biocompatibility of RCP[25-26]. Therefore, we propose the novel strategy for the innovated scaffold in bone tissue engineering approach using RCP and nanoparticulated β-TCP. Accordingly, we created and characterized the RCP scaffold applied with β-TCP

nanoparticles (RCP-TCP) regarding cellular behaviors in vitro. Furthermore, bone formation of rat cranial bone defect following implantation of RCP-TCP was assessed in vivo. We hypothesized that RCP-TCP exhibited the great biosafety and bone-forming ability.

Materials and Methods

Preparation of RCP-TCP

β-TCP (β-TCP-100, Taihei Chemical Industrial Co., Ltd., Osaka, Japan) was prepared by described previously[27]. Nanoparticulated β-TCP was fabricated by Nanovater (NVL-AS200-D10, Yoshida Kikai Co., Ltd., Nagoya, Japan) and dispersed into water (10 wt%). Particle size of β-TCP was measured by particle size distribution measuring apparatus (SALD-2100, Shimadzu Corp., Kyoto, Japan). RCP was provided by FUJIFILM Corp. (Fuji bone graft, Tokyo, Japan). Collagen type I-based recombinant peptide (cellnest™, FUJIFILM Corp.) was thermal-crosslinked and pulverized to obtain RCP. Subsequently, 500 μL of β-TCP dispersion (concentrations; 0, 0.01, 0.1, 1 and 10 wt%) was added into 100 mg freeze-dried RCP, and then designated as RCP, RCP-0.01TCP, RCP-0.1TCP, RCP-1TCP and RCP-10TCP, respectively.

Characterization of RCP-TCP

Each sample was analyzed using a scanning electron microscope (SEM, S-4000; Hitachi, Ltd., Tokyo, Japan) at an accelerating voltage of 10 kV after coating with a thin layer of Pt-Pd. In addition, samples were characterized using energy dispersive X-ray spectrometry (EDX, JSM-6500F, JEOL Ltd., Tokyo, Japan).

Assessments of cytocompatibility of RCP-TCP

Mouse osteoblastic MC3T3-E1 cells (RIKEN BioResource Center, Tsukuba, Japan) were seeded (1×10^4 cells/ 0.5 mL/ well) and cultured on the samples (100 mg) in humidified atmosphere containing 5% CO_2 at 37 °C using 48-well cell culture plates with culture medium (MEM alpha, GlutaMAX-I, Thermo Fisher Scientific, Waltham, MA, USA) supplemented with 10% fetal bovine serum (Qualified FBS, Thermo Fisher Scientific) and 1% antibiotics (Penicillin-Streptomycin, Thermo Fisher Scientific).

The assessments of cell proliferation and cytotoxicity were carried out using assay kits of water-soluble tetrazolium salt (WST) -8 (Cell Counting Kit-8, Dojindo Laboratories, Mashiki, Japan) and a lactate dehydrogenase (LDH, Cytotoxicity LDH Assay Kit-WST, Dojindo Laboratories), respectively. The absorbance at 450 nm (WST-8) and 490 nm (LDH) was measured using a microplate reader (Multiskan FC, Thermo

Fisher Scientific). For the cell adhesion assay, cells cultured for 24 hours were washed with phosphate-buffered saline (PBS, FUJIFILM Wako Pure Chemical Corp., Osaka, Japan) and fixed with 3.5% formaldehyde. A staining solution was prepared by dissolving phalloidin (1.5 μg, Actistain 555 Fluorescent Phalloidin, Cytoskeleton Inc., Denver, CO, USA) and 4' ,6-diamidino-2-phenylindole (2 μg, Dojindo Laboratories) in 500 μL of a bovine serum albumin (BSA, 7.5% w/v Albumin Dulbecco's-PBS (−) Solution from bovine serum, FUJIFILM Wako Pure Chemical Corp.). The samples were immersed in this solution overnight at 4 °C to stain cultured cells and then washed with PBS. The stained cells were observed using a fluorescence microscope (Biorevo BZ-9000, Keyence Corp., Osaka, Japan). Some samples were stained using the LIVE/DEAD Viability/Cytotoxicity Kit for mammalian cells (Thermo Fisher Scientific), following the manufacturer's instructions. Stained samples were also examined using a fluorescence microscope.

Assessments of osteoblastic differentiation to RCP-TCP

MC3T3-E1 cells were seeded (1×10^6 cells/ 0.5 mL/ well) were grown on the samples (100 mg) in 48-well plates. Medium exchange performed every 2 days. The cells cultured for 14 days were washed with PBS and fixed with 3.5% formaldehyde. They

were stained with 3 μL of DAPI solution (Dojindo Laboratories) and 5 μL of Alexa Fluor® 488-labeled anti-runt-related transcription factor 2 (Runx2) antibody (Abcam, Cambridge, UK) dissolved in 500 μL of BSA for 12 hours at 4 °C. The stained cells were observed using a fluorescence microscope.

In addition, total RNA of cultured cells was extracted using Trizol (Invitrogen, Carlsbad, CA, USA) according to the manufacturer's instructions. Reverse transcription was conducted with 1 μg of RNA to obtain cDNA. The cDNA was amplified by Rever Tra Ace-α FSK-101 (Toyobo Co., Ltd., Osaka, Japan). Real-time PCR (ABI Prism 7300 sequence detection system, Applied Biosystems, Carlsbad, CA, USA) was performed using primers (Applied Biosystems) for the following genes were used: Runx2 (Mm00501584_m1), Alpl (Mm00475834_m1), Ibsp (Mm00492555_m1) and glyceraldehyde-3-phosphate dehydrogenase (GAPDH, Mm99999915_g1). Data obtained for each sample were standardized against the expression of GAPDH and were calculated using the 2-ΔΔCt method[28-29].

Animal surgery

Thirty-six 10-week-old male Wistar rats weighing approximately 190–210 g were used for this experiment. The in vivo experiments in rats were carried out in accordance

with the institutional animal use and care regulations of Hokkaido University (Animal Research Committee of Hokkaido University, Approval number 16-29) and approved by the Animal Research Committee of Hokkaido University. Surgical procedures were performed under general anesthesia by intraperitoneal injection of medetomidine hydrochloride (0.15 mL/kg, Domitor, Nippon Zenyaku Kogyo Co., Ltd., Koriyama, Japan), Midazolam (0.4 mL/kg, Dormicum, Astellas Pharma Inc., Tokyo, Japan), butorphanol tartrate (0.5 mL/kg, Vetorphale, Meiji Seika Pharma Co., Ltd., Tokyo, Japan) and local injection of 2 % lidocaine hydrochloride with 1 : 80,000 epinephrine (Xylocaine Cartridge for Dental Use, Dentsply Sirona K.K., Tokyo, Japan).

After elevation of skin-periosteal flap, bone defects with a 4.5 mm diameter were created on the cranial bone with a trephine bar (Meis Trephine bar, Hager & Meisinger GmbH, Neuss, Germany) operating at 1500 rpm/min or less. Subsequently, defects are filled with RCP or RCP-1TCP (4 mg / defect). No implantation was performed as the negative control. After that, skin was sutured (BioFit-D 4-0; Washiesu Medical Corp., Tokyo, Japan) and applied with tetracycline hydrochloride (Achromycin ointment; Pola Pharma Inc., Tokyo, Japan) to prevent postoperative infection.

Assessments of bone forming effect of RCP-TCP in rat cranial bone

At 2 and 4 weeks post-surgery, rats were euthanized using an overdose of sodium pentobarbital (2.0 mL/kg, Somnopentyl; Kyoritsu Seiyaku Corp., Tokyo, Japan). The samples were assessed by X-ray computed tomography scanner (Latheta LCT-200, Hitachi, Ltd.). From the captured CT images, the radiolucent area of cranial bone was measured by software package (ImageJ 1.41; National Institutes of Health, Bethesda, MD, USA).

To assess the histological analyses, samples were fixed in 10% buffered formalin, decalcified by 10 % ethylenediaminetetraacetic acid and embedded in paraffin. After thin slicing (5 μm), sections were stained with hematoxylin and eosin and observed using light microscopy (BX53, Olympus Corp., Tokyo, Japan). After the length of the bone defect (L) and new bone (NB) was measured by software package, bone formation rate (NB / L %) was calculated.

Statistical analysis

The means and standard deviations of each parameter were calculated for each group. Differences between the groups were analyzed using one-way ANOVA with multiple comparisons. *P*-values < 0.05 was statistically significant. All statistical

procedures were performed using a software package (SPSS 11.0, IBM Corp., Armonk, NY, USA).

Results

Characterization of RCP-TCP

RCP showed the granular shape with 1 mm thickness (Fig. 1A). Particle distribution measurement showed that average particle size of β-TCP was approximately 700 nm. The SEM images of RCP-TCP was shown that β-TCP nanoparticles dose-dependently covered to the surface of RCP. In RCP-10TCP, the surface of the RCP was fully covered by a layer of aggregated β-TCP nanoparticles (Figs. 1B-F). EDX mapping analysis of surface of RCP-TCP confirmed the presence of elements; P and Ca (Fig. 2). The intensity of P and Ca dose-dependently increased.

Cytocompatibility of RCP-TCP

The results of WST-8 and LDH assays are presented. All sample revealed the WST-8 increase from 3 to 7 days. RCP-1TCP exhibited great WST-8 activity at 7 days and significant difference compared to other groups (Fig. 3A). In addition, LDH activity of RCP-TCP was comparable or low to RCP group through experimental periods. Cell

cytotoxicity of RCP-1TCP at 7 days were significantly less than RCP (Fig. 3B).

Cultured cell of all samples expressed actin as the evidence of cell attachment and spreading, regardless of application of β-TCP nanoparticles. In addition, the LIVE/DEAD BacLight assay showed that all samples consistently exhibited live cells stained green fluorescence (Fig. 3C).

Assessments of osteoblastic differentiation

Immunostaining of osteoblastic MC3T3-E1 cells seeded to RCP-1TCP showed the green fluorescence related to Runx2 expression (Fig. 4A). Measurements of amplified cDNA by real-time RT-PCR demonstrated that RCP and RCP-1TCP were significantly higher than control (no application) in osseous markers; Runx2, alkaline phosphatase (ALP) and bone sialoprotein (BSP). No significant difference was found between RCP and RCP-1TCP (Figs. 4B-D).

Assessment of bone formation by CT image

CT images at 2 and 4 weeks after surgery were shown in Fig. 5A. At 2 weeks, the radiopacity area of cranial bone created by trephine bur was rarely observed in control. In contrast, RCP and RCP-1TCP groups exhibited to increase the radiopacity. At 4 weeks,

control specimens had slight radiopacity area, similar to 2 weeks sample. While, RCP and RCP-1TCP demonstrated that radiopacity area was remarkable and frequently appeared at the center region of the bone defect. To compare the increase of radiopacity area, radiolucency area was measured by software. At 2 weeks after surgery, radiolucency of RCP-1TCP was significantly lower than those of control and RCP. The decrease of radiolucency of RCP, as well as RCP-1TCP, was remarkably proceeded at 4 weeks and significant differences were found compared to control (Fig. 5B).

Histological evaluation of bone formation

Histological specimens of control (no implantation) at 2 weeks revealed that bone defect was filled with connective tissue and rarely observed new bone formation. In RCP and RCP-1TCP groups, implanted RCP, resembling mesh structure, were observed to remain in the defect and slight new bone was formed around RCP (Fig. 6).

In control group at 4 weeks, new bone formation was slight, similar to 2 weeks control sample. In RCP and RCP-1TCP applied groups at 4 weeks, bone formation was remarkable, when compared to control. In particular, RCP-1TCP implantation showed the large amount of new bone to fully occupy the defect. Bone tissue was deposited along with strut of RCP to fill the meshwork structure (Fig. 7).

Measurements of bone formation rate revealed that RCP-1TCP significantly increased compared with control and RCP groups at 2 and 4 weeks. In addition, RCP at 4weeks was significantly greater than control (Fig. 8).

Discussion

From the evidences of SEM observation and EDX analysis, β-TCP nanoparticles dose-dependently adhered to RCP to exhibit the excellent biocompatibility. In particular, coating of β-TCP nanoparticles on the RCP surface promoted WST-8 activity, or osteoblastic cell proliferation. Thus, it was suggested that application of β-TCP nanoparticles exerted the positive effects on cyto-compatibility. It was reported that the material surface properties including surface roughness, charge and hydrophilicity, may affect the ability of cell adhesion[30-31]. We supposed that nano-modification with nanoparticulated substances increased the total surface area and subsequent adsorption of signaling molecules to promote the cell behaviors[32]. Some previous reports using bovine collagen showed a similar trend, that is, nanostructured scaffold enhanced cell proliferation[33-34]. Thus, the bone induction would be anticipated by the cell proliferative ability of nanomodified RCP. While, Murakami et al. reported that application of large amounts of β-TCP nanoparticles caused severe inflammatory response at early wound

healing stage[17]. Hence, the application dose of nano substances need to be investigated in detail.

RCP-1TCP promoted the expression of osteogenic markers, such as Runx2, ALP and BSP. Runx2 protein stimulates the differentiation of multipotent mesenchymal cells into immature osteoblasts[35]. ALP and BSP, related to mineralization process, were osteogenic markers to detect the mature osteoblast. Therefore, RCP-1TCP would possess the potential of bone induction via osteoblastic cell differentiation. In addition, RCP alone stimulated the induction of these osseous markers. Since we could not find the significant differences of mRNA expression between RCP and RCP-1TCP, osteoblastic differentiation might be resulted by the capability of RCP, not applied β-TCP nanoparticles. Collagen type I-based recombinant peptide includes many RGD motif to stimulate cell adhesion via integrin binding[24]. It is well-known that integrin-extracellular-matrix adhesion-mediated signaling pathways would be essential for osteoblastic differentiation[36]. Jikko et al. reported that integrin receptors of collagen regulated the response to bone morphogenetic protein-2 to obtain the regulation of ALP mRNA[37]. Schwab et al. revealed that the osteogenic differentiation of mesenchymal stem cells was upregulated by RGD-containing extracellular matrix[38]. Hence, great bone inductive effect of RCP-applied biomaterials would be convenient for bone tissue engineering

strategy.

In the assessments of bone formation in rat at 2 weeks, RCP-1TCP significantly stimulated the formation of bone tissue compared to RCP and control. Since RCP alone showed great bone formation at 4 weeks, application of β-TCP nanoparticles to RCP might accelerate the bone formation even initial stage caused by cell proliferative ability of β-TCP nanoparticles. In general, β-TCP application provides Ca/P ion to regenerative regions resulted in resorption by phagocytosis[39-40]. Reportedly, Ca and P stimulated the expression of osseous markers in osteoblastic cells to adjust the in vivo environment for bone generation[41]. In addition, nano-ceramics exhibits high biodegradability when implanted in the body[42]. In this experiment, residual β-TCP rarely found in histological specimens at 2 weeks, thereby suggesting that β-TCP nanoparticles appeared to be well-degraded to create the effects of osteoconductivity immediately after implantation. While, at 4 weeks, RCP and RCP-1TCP consistently enhanced the bone tissue formation. From these evidences, RCP-1TCP exhibited two biological outcomes; proliferation and differentiation of cells, to consequently facilitate the bone formation. We supposed that osteoconductive effect of RCP would be comparable to RCP-1TCP if the long-term experimental observation. Early bone healing of RCP-1TCP should provide the great advantages for the tissue stability in bone tissue engineering therapy.

Conclusion

We assessed the cytocompatibility and bone-forming ability of RCP applied with β-TCP nanoparticles. The results showed that the application of β-TCP nanoparticles exhibited cyto-compatibility and promoted the proliferative activity of osteoblastic cell. Real-time RT-PCR examination showed that RCP stimulated the osteogenic differentiation regardless of the application of β-TCP nanoparticles. In rat experiments, RCP-1TCP significantly showed the bone formation through experimental periods, when compared to control (no application) and RCP. Hence, the osteogenic capability of RCP-1TCP would be beneficial for application to bone tissue engineering therapy.

Acknowledgments

The authors thank FUJIFILM Corp. for providing Fuji bone graft and Taihei Chemical Industrial Co., Ltd., for providing nanoparticulated β-TCP. This work was supported by JPSP KAKENHI Grant Numbers JP16K11822 and JP18K17038 and AMED translational research program. The authors report that they have no conflict of interest related to this study.

References

1) O'Keefe RJ, Mao J. Bone tissue engineering and regeneration: from discovery to the clinic - an overview. Tissue Eng Part B Rev 17 : 389-392, 2011.

2) Titorencu I, Albu MG, Nemecz M, Jinga VV. Natural polymer-cell bioconstructs for bone tissue engineering. Curr Stem Cell Res Ther 12 : 165-174, 2017.

3) Liu Q, Wang J, Chen Y, Zhang Z, Saunders L, Schipani E, Chen Q, Ma PX. Suppressing mesenchymal stem cell hypertrophy and endochondral ossification in 3D cartilage regeneration with nanofibrous poly (l-lactic acid) scaffold and matrilin-3. Acta Biomater 76 : 29-38, 2018.

4) Fawzy El-Sayed KM, Mekhemar MK, Beck-Broichsitter BE, Bähr T, Hegab M, Receveur J, Heneweer C, Becker ST, Wiltfang J, Dörfer CE. Periodontal regeneration employing gingival margin-derived stem/progenitor cells in conjunction with IL-1ra-hydrogel synthetic extracellular matrix. J Clin Periodontol 42 : 448-457, 2015.

5) Li J, Zhang X, Guo Q, Zhang J, Cao Y, Zhang X, Huang J, Wang Q, Liu X, Hao C. Preparation and in vitro evaluation of tissue engineered osteochondral integration of multi-layered scaffold. Zhongguo Xiu Fu Chong Jian Wai Ke Za Zhi 32 : 434-440, 2018.

6) Wang T, Guo S, Zhang H. Synergistic effects of controlled-released BMP-2 and VEGF

from nHAC/PLGAs scaffold on osteogenesis. Biomed Res Int 2018 : 3516463, 2018.

7) Sofi HS, Ashraf R, Beigh MA, Sheikh FA. Scaffolds fabricated from natural polymers/composites by electrospinning for bone tissue regeneration. Adv Exp Med Biol 1078 : 49-78, 2018.

8) Carrel JP, Wiskott A, Moussa M, Rieder P, Scherrer S, Durual S. A 3D printed TCP/HA structure as a new osteoconductive scaffold for vertical bone augmentation. Clin Oral Implants Res 27 : 55-62, 2016.

9) Ibara A, Miyaji H, Fugetsu B, Nishida E, Takita H, Tanaka S, Sugaya T, Kawanami M. Osteoconductivity and biodegradability of collagen scaffold coated with nano-β-TCP and fibroblast growth factor 2. J Nanomater : 639502, 2013.

10) Yoshida T, Miyaji H, Otani K, Inoue K, Nakane K, Nishimura H, Ibara A, Shimada A, Ogawa K, Nishida E, Sugaya T, Sun L, Fugetsu B, Kawanami M. Bone augmentation using a highly porous PLGA/b-TCP scaffold containing fibroblast growth factor-2. J Periodontal Res 50 : 265-273, 2015.

11) Kawamoto K, Miyaji H, Nishida E, Miyata S, Kato A, Tateyama A, Furihata T, Shitomi K, Iwanaga T, Sugaya T. Characterization and evaluation of graphene oxide scaffold for periodontal wound healing of class II furcation defects in dog. Int J Nanomedicine 13 : 2365-2376, 2018.

12) Kosen Y, Miyaji H, Kato A, Sugaya T, Kawanami M. Application of collagen hydrogel/sponge scaffold facilitates periodontal wound healing in class II furcation defects in beagle dogs. J Periodontal Res 47 : 626-634, 2012.

13) Nishida E, Miyaji H, Takita H, Kanayama I, Tsuji M, Akasaka T, Sugaya T, Sakagami R, Kawanami M: Graphene oxide coating facilitates the bioactivity of scaffold material for tissue engineering. Jpn J Appl Phys 53 : 06JD04, 2014.

14) Park KS, Kim BJ, Lih E, Park W, Lee SH, Joung YK, Han DK. Versatile effects of magnesium hydroxide nanoparticles in PLGA scaffold-mediated chondrogenesis. Acta Biomater 73 : 204-216, 2018.

15) Chamieh F, Collignon AM, Coyac BR, Lesieur J, Ribes S, Sadoine J, Llorens A, Nicoletti A, Letourneur D, Colombier ML, Nazhat SN, Bouchard P, Chaussain C, Rochefort GY. Accelerated craniofacial bone regeneration through dense collagen gel scaffolds seeded with dental pulp stem cells. Sci Rep 6 : 38814, 2016.

16) Wang Y, Van Manh N, Wang H, Zhong X, Zhang X, Li C. Synergistic intrafibrillar/extrafibrillar mineralization of collagen scaffolds based on a biomimetic strategy to promote the regeneration of bone defects. Int J Nanomedicine 11 : 2053-2067, 2016.

17) Murakami S, Miyaji H, Nishida E, Kawamoto K, Miyata S, Takita H, Akasaka T,

Fugetsu B, Iwanaga T, Hongo H, Amizuka N, Sugaya T and Kawanami M. Dose effects of beta-tricalcium phosphate nanoparticles on biocompatibility and bone conductive ability of three-dimensional collagen scaffolds. Dental Materials J 36(5) : 573-583, 2017.

18) Wei B, Zhai Z, Wang H, Zhang J, Xu C, Xu Y, He L, Xie D. Graphene-oxide-based FRET platform for sensing xenogeneic collagen coassembly. J Agric Food Chem 66(34) : 9080-9086, 2018.

19) Iwama R, Anada T, Shiwaku Y, Tsuchiya K, Takahashi T, Suzuki O. Osteogenic cellular activity around onlaid octacalcium phosphate-gelatin composite onto rat calvaria. J Biomed Mater Res A 106(5) : 1322-1333, 2018.

20) Ogawa K, Miyaji H, Kato A, Kosen Y, Momose T, Yoshida T, Nishida E, Miyata S, Murakami S, Takita H, Fugetsu B, Sugaya T, Kawanami M. Periodontal tissue engineering by nano beta-tricalcium phosphate scaffold and fibroblast growth factor-2 in one-wall infrabony defects of dogs. J Periodontal Res 51(6) : 758-767, 2016.

21) Carfì Pavia F, Conoscenti G, Greco S, La Carrubba V, Ghersi G, Brucato V. Preparation, characterization and in vitro test of composites poly-lactic acid/hydroxyapatite scaffolds for bone tissue engineering. Int J Biol Macromol 119 : 945-953, 2018.

22) Kira T, Akahane M, Omokawa S, Shimizu T, Kawate K, Onishi T, Tanaka Y. Bone regeneration with osteogenic matrix cell sheet and tricalcium phosphate: An experimental study in sheep. World J Orthop 8(10) : 754-760, 2017.

23) Remya KR, Joseph J, Mani S, John A, Varma HK, Ramesh P. Nanohydroxyapatite incorporated electrospun polycaprolactone/polycaprolactone-polyethyleneglycol-polycaprolactone blend scaffold for bone tissue engineering applications. J Biomed Nanotechnol 9(9) : 1483-1494, 2013.

24) Pawelec KM, Confalonieri D, Ehlicke F, van Boxtel HA, Walles H, Kluijtmans SGJM. Osteogenesis and mineralization of mesenchymal stem cells in collagen type I-based recombinant peptide scaffolds. J Materials Research 105(7) : 1856-1866, 2017.

25) Miyamoto M, Nakamura K, Shichinohe H, Yamauchi T, Ito M, Saito H, Kawabori M, Osanai T, Sasaki T, Houkin K, Kuroda S. Human recombinant peptide sponge enables novel, less invasive cell therapy for ischemic stroke. Stem Cells Int 2018 : 4829534, 2018.

26) Mashiko T, Takada H, Szu‐Hsien Wu, Kanayama K, Jingwei Feng, Tashiro K, Asahi R, Sunaga A, Hoshi K, Kurisaki A, Takato T, Yoshimura K. Therapeutic effects of a recombinant human collagen peptide bioscaffold with human adipose‐derived stem cells on impaired wound healing after radiotherapy. J Tissue Engineering and

Regenerative Medicine 12(5) : 1186-1194, 2018.

27) Inomata Y, Okano H, Watanabe S, Nakagawa S. Evaluation of powder property of calcium phosphate. Phosphorus Research Bulletin 32 : 017-021, 2016.

28) Pfaffl MW. A new mathematical model for relative quantification in real-time RT-PCR. Nucleic Acids Res 29 : e45, 2001.

29) Schmittgen TD, Zakrajsek BA. Effect of experimental treatment on housekeeping gene expression: validation by real-time, quantitative RT-PCR. J Biochem Biophys Methods 46 : 69–81, 2000.

30) Webb K, Hlady V, Tresco PA. Relative importance of surface wettability and charged functional groups on NIH 3T3 fibroblast attachment, spreading, and cytoskeletal organization. J Biomed Mater Res 41(3) : 422-430, 1998.

31) Feller L, Jadwat Y, Khammissa RA, Meyerov R, Schechter I, Lemmer J. Cellular responses evoked by different surface characteristics of intraosseous titanium implants. Biomed Res Int 2015 : 171945, 2015.

32) Roozbahani M, Alehosseini M, Kharaziha M, Emadi R. Nano calcium phosphate bone cement based on Si-stabilized α-tricalcium phosphate with improved mechanical properties. Mater Sci Eng C Mater Biol Appl 81 : 532-541, 2017.

33) Ebrahimi M, Pripatnanont P, Suttapreyasri S, Monmaturapoj N. In vitro biocompatibility analysis of novel nano-biphasic calcium phosphate scaffolds in different composition ratios. J Biomed Mater Res B Appl Biomater 102(1) : 52-61, 2014.

34) Kankilic B, Köse S, Korkusuz P, Timuçin M, Korkusuz F. Mesenchymal stem cells and nano-bioceramics for bone regeneration. Curr Stem Cell Res Ther 11(6) : 487-493, 2016.

35) An J, Yang H, Zhang Q, Liu C, Zhao J, Zhang L, Chen B. Natural products for treatment of osteoporosis: The effects and mechanisms on promoting osteoblast-mediated bone formation. Life Sci 147 : 46-58, 2016.

36) G.B. Schneider, R. Zaharias, C. Stanford. Osteoblast integrin adhesion and signaling regulate mineralization. J Dent Res 80(6) : 1540-1544, 2001.

37) Jikko A1, Harris SE, Chen D, Mendrick DL, Damsky CH. Collagen integrin receptors regulate early osteoblast differentiation induced by BMP-2. J Bone Miner Res 14(7) : 1075-83, 1999.

38) Schwab EH, Halbig M, Glenske K, Wagner AS, Wenisch S, Cavalcanti-Adam EA. Distinct effects of RGD-glycoproteins on integrin-mediated adhesion and osteogenic

differentiation of human mesenchymal stem cells. Int J Med Sci 10(13) : 1846-59, 2013.

39) Eftekhari H, Farahpour MR, Rabiee SM. Histopathological evaluation of potential impact of β-tricalcium phosphate (HA+ β-TCP) granules on healing of segmental femur bone defect. Bratisl Lek Listy 116(1) : 30-34, 2015.

40) Oztürk A, Yetkin H, Memis L, Cila E, Bolukbasi S, Gemalmaz C.Demineralized bone matrix and hydroxyapatite/tri-calcium phosphate mixture for bone healing in rats. Int Orthop 30(3) : 147-152, 2006.

41) Park H, Kim JS, Oh EJ, Kim TJ, Kim HM, Shim JH, Yoon WS, Huh JB, Moon SH, Kang SS, Chung HY. Effects of three-dimensionally printed polycaprolactone/β-tricalcium phosphate scaffold on osteogenic differentiation of adipose tissue- and bone marrow-derived stem cells. Arch Craniofac Surg 19(3) : 181-189, 2018.

42) Cao L, Chen Q, Jiang LB, Yin XF, Bian C, Wang HR, Ma YQ, Li XQ, Li XL, Dong J. Bioabsorbable self-retaining PLA/nano-sized β-TCP cervical spine interbody fusion cage in goat models: an in vivo study. Int J Nanomedicine 12 : 7197-7205, 2017.

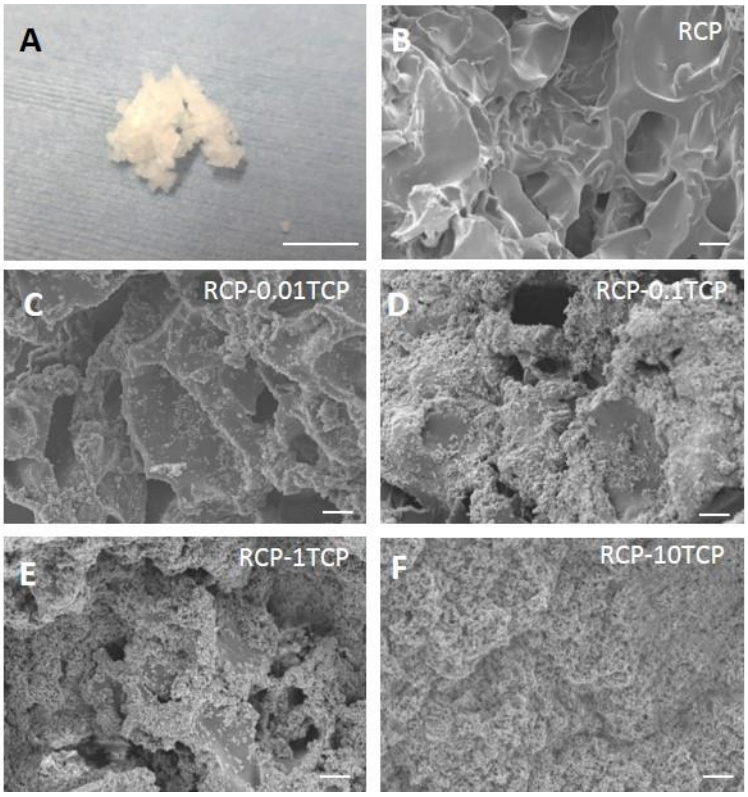

Fig 1

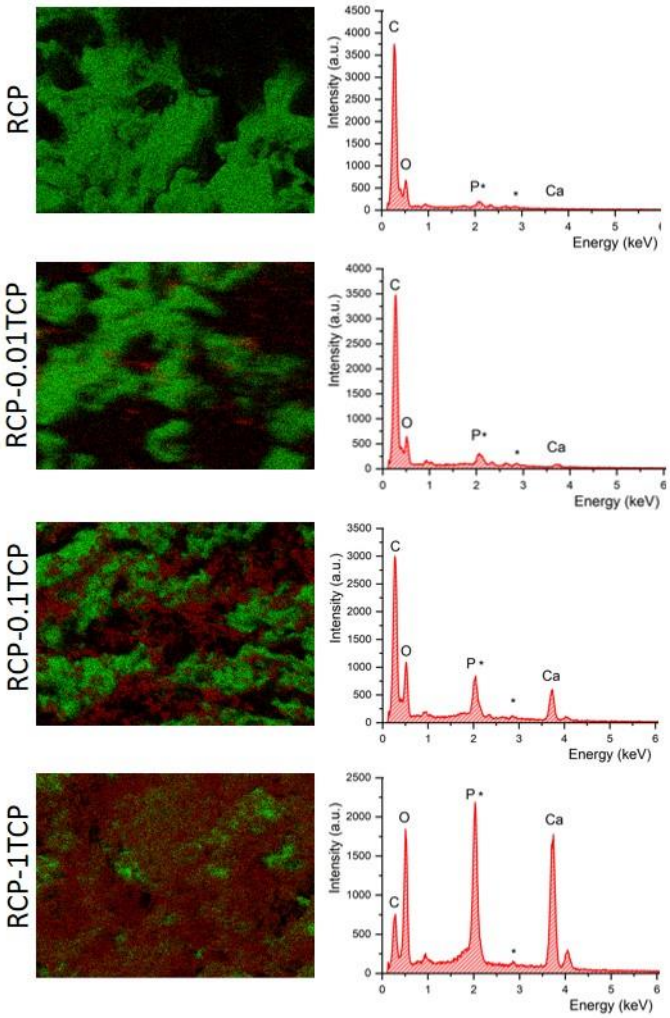
RCP
RCP-0.01TCP
RCP-0.1TCP
RCP-1TCP
Intensity (a.u.)
Energy (keV)
C
O
P
Ca

Fig 2

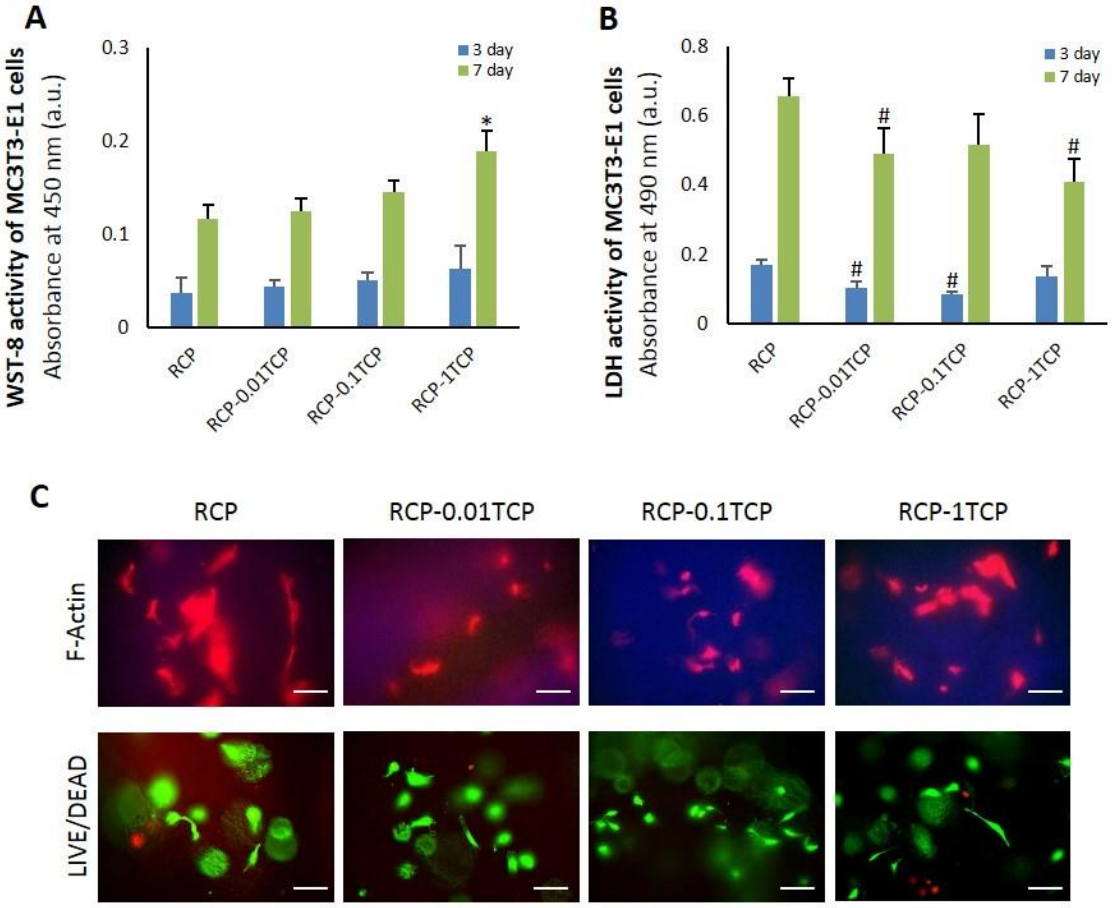
A
WST-8 activity of MC3T3-E1 cells
Absorbance at 450 nm (a.u.)
0.3
0.2
0.1
0
3 day
7 day
*
RCP
RCP-0.01TCP
RCP-0.1TCP
RCP-1TCP
B
LDH activity of MC3T3-E1 cells
Absorbance at 490 nm (a.u.)
0.8
0.6
0.4
0.2
0
3 day
7 day
#
#
#
#
RCP
RCP-0.01TCP
RCP-0.1TCP
RCP-1TCP
C
RCP
RCP-0.01TCP
RCP-0.1TCP
RCP-1TCP
F-Actin
LIVE/DEAD

Fig 3

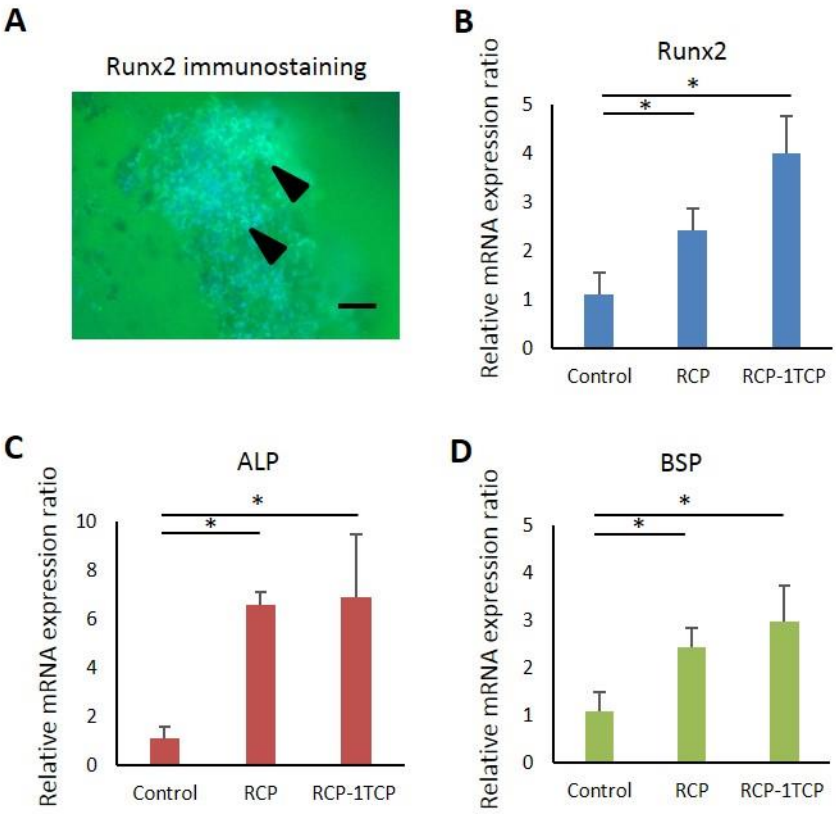
A
Runx2 immunostaining
B
Runx2
Relative mRNA expression ratio
0
1
2
3
4
5
*
*
Control
RCP
RCP-1TCP
C
ALP
Relative mRNA expression ratio
0
2
4
6
8
10
*
*
Control
RCP
RCP-1TCP
D
BSP
Relative mRNA expression ratio
0
1
2
3
4
5
*
*
Control
RCP
RCP-1TCP

Fig 4

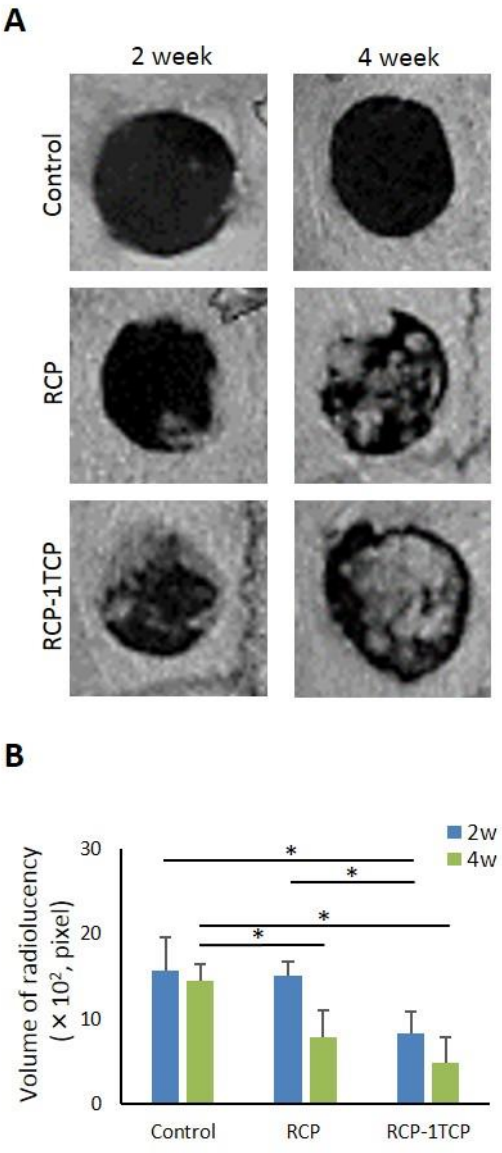
A
2 week
4 week
Control
RCP
RCP-1TCP
B
2w
4w
Volume of radiolucency
(× 10², pixel)
30
20
10
0
*
*
*
*
Control
RCP
RCP-1TCP

Fig 5

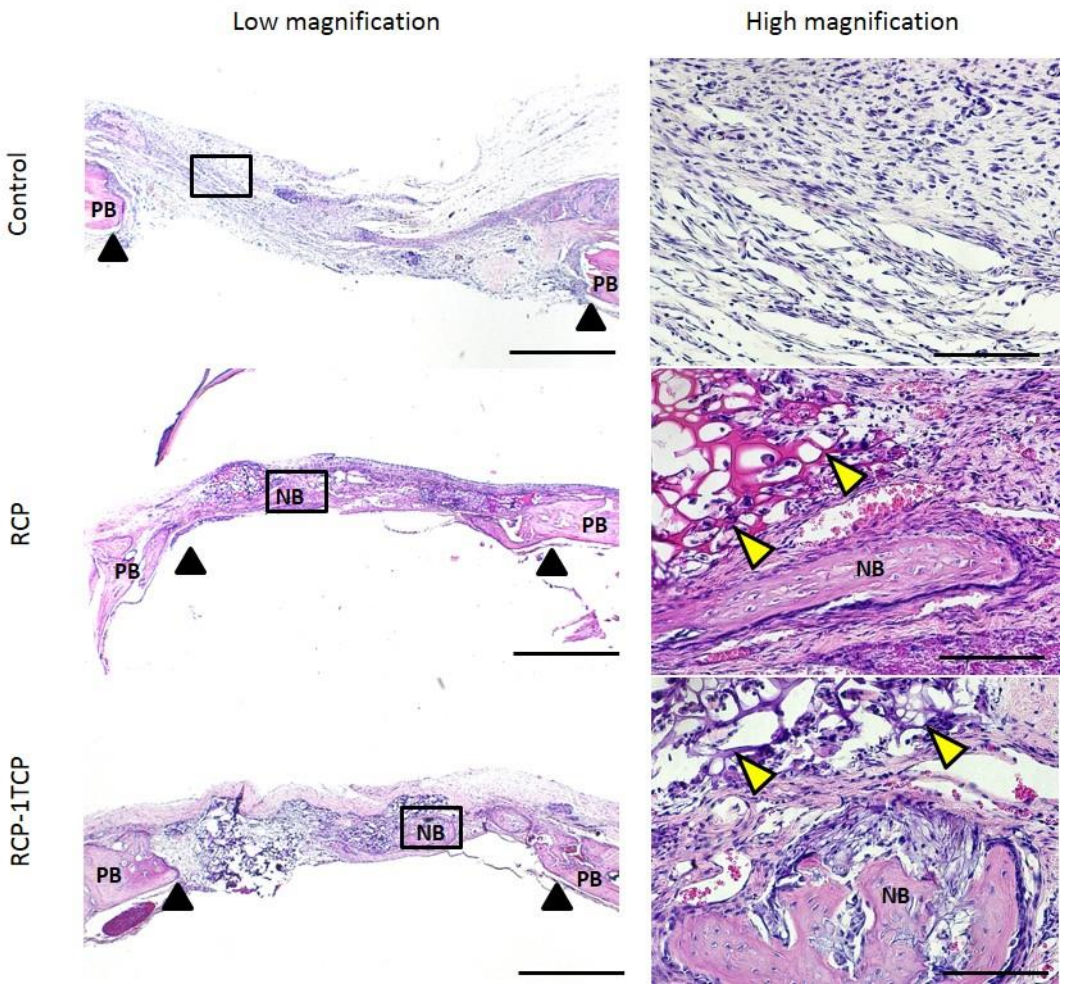
Low magnification
High magnification
Control
RCP
RCP-1TCP
PB
PB
NB
PB
PB
NB
PB
PB
NB

Fig 6

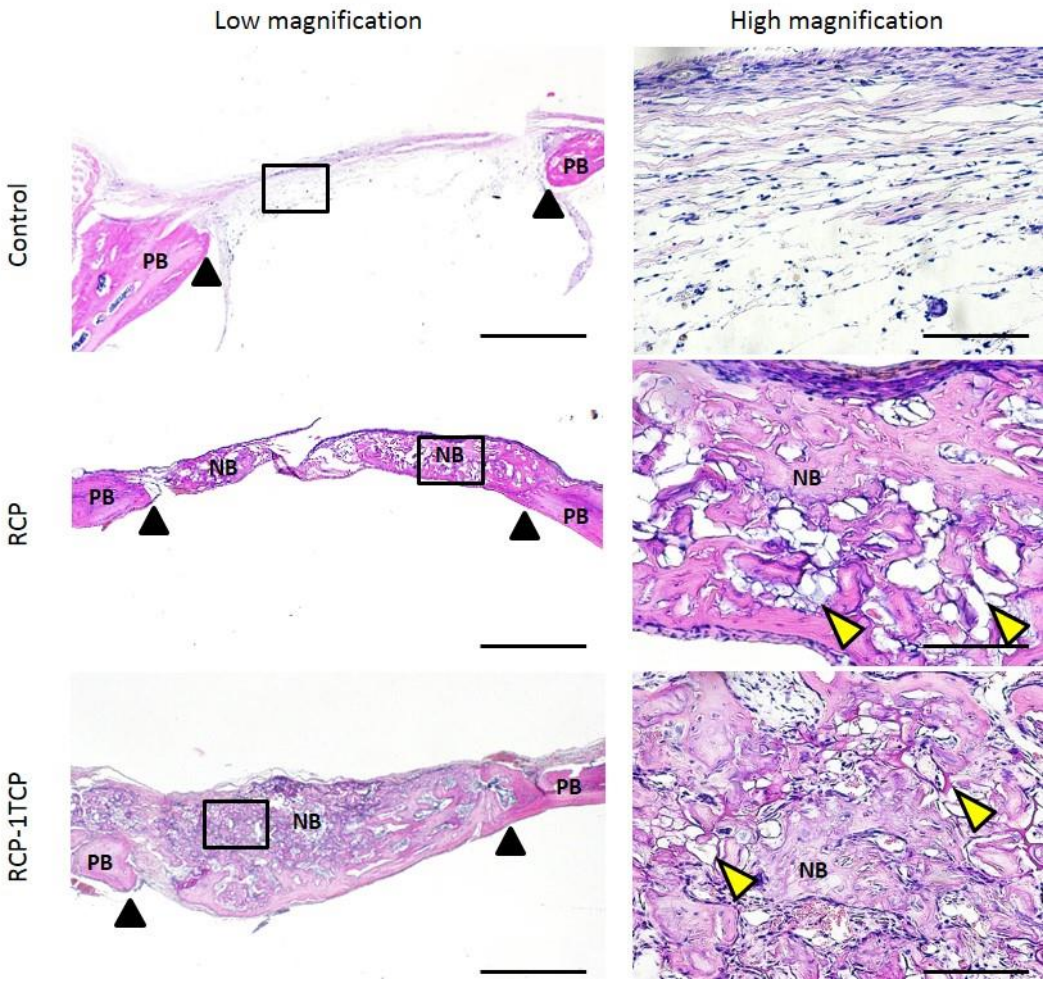
Low magnification
High magnification
Control
RCP
RCP-1TCP
PB
NB

Fig 7

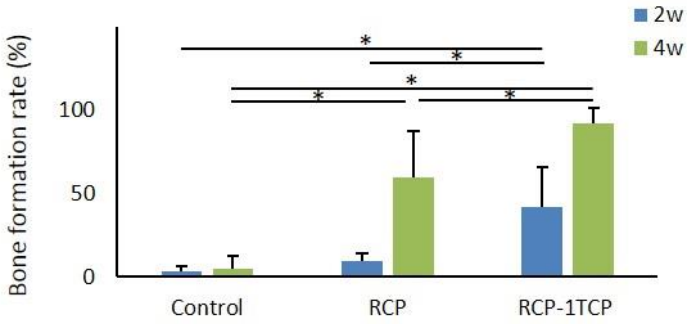

Fig 8

Figure legends

Figure 1. Digital photograph and SEM images of RCP-TCP

(A) Digital photograph of RCP-1TCP. (B-F) SEM images of RCP (B), RCP-0.01TCP (C), RCP-0.1TCP (D), RCP-1TCP (E) and RCP-10TCP (F). Scale bar represents 10 mm (A), 10 μm (B-F).

Abbreviations: RCP, recombinant human collagen-peptide based scaffold; TCP, tricalcium phosphate; SEM, scanning electron microscope.

Figure 2. EDX mapping of RCP-TCP

The elements; Ca and C, were stained in red and green, respectively.

Abbreviations: EDX, energy dispersive X-ray spectrometry; RCP, recombinant human collagen-peptide based scaffold; TCP, tricalcium phosphate.

Figure 3. Assessments of cytocompatibility of RCP-TCP

(A)WST-8 activity of MC3T3-E1 cells (N=4, mean ± SD). *: $P<0.05$, vs. RCP, RCP-0.01TCP and TCP-0.1RCP. (B) LDH activity of MC3T3-E1 cells (N=4, mean ± SD). #: $P<0.05$, vs RCP. (C) Microscopic images of F-actin and LIVE/DEAD BacLight staining of MC3T3-E1 cells after 24 hours incubation. Scale bar represents 100 μm.

Abbreviations: WST-8, water-soluble tetrazolium salts-8; RCP, recombinant human collagen-peptide based scaffold; TCP, tricalcium phosphate; LDH, lactate dehydrogenase.

Figure 4. Assessments of osteoblastic differentiation related to RCP-TCP

(A) Runx2 immunostaining of RCP-1TCP. Scale bar represents 100 μm. Arrowhead shows the cellular expression of Runx2 on the RCP-1TCP. (B-D) Measurements of amplified cDNA of Runx2 (B), ALP (C) and BSP (D) by RT-PCR (N=4, mean ± SD). *: $P<0.05$.

Abbreviations: ALP, alkaline phosphatase; BSP, bone sialoprotein; RCP, recombinant human collagen-peptide based scaffold; RT-PCR, reverse transcription polymerase chain reaction; Runx2, runt-related transcription factor 2; TCP, tricalcium phosphate.

Figure 5. CT analyses of implanted RCP-TCP in rat

(A) CT images of control, RCP and RCP-1TCP groups at 2 and 4 weeks post-surgery. (B) Volume of radiolucency at 2 and 4 weeks (N=6, mean ± SD). *: $P<0.05$.

Abbreviations: CT, computed tomography; RCP, recombinant human collagen-peptide based scaffold; TCP, tricalcium phosphate.

Figure 6. Histological findings at 2 weeks after implantation in rat

Specimens receiving control, RCP and RCP-1TCP. High magnification images related to flamed area in low magnification images. Scale bar represents 1 mm (low magnification) and 100 μm (high magnification). Yellow arrowheads indicate the residual implanted scaffold. Black arrowheads indicate the border of the bone defect. Staining: hematoxylin and eosin.

Abbreviations: NB, new bone; PB, preexisting bone; RCP, recombinant human collagen-peptide based scaffold; TCP, tricalcium phosphate.

Figure 7. Histological findings at 4 weeks after implantation in rat

Specimens receiving control, RCP and RCP-1TCP at 4 weeks. High magnification images related to flamed area in low magnification images. Scale bar represents 1 mm (low magnification) and 100 μm (high magnification). Yellow arrowheads indicate the residual implanted scaffold. Black arrowheads indicate the border of the bone defect. Staining: hematoxylin and eosin.

Abbreviations: NB, new bone; PB, preexisting bone; RCP, recombinant human collagen-peptide based scaffold; TCP, tricalcium phosphate.

Figure 8. Histomorphometric measurements of newly formed bone

Bone formation rate at 2 and 4 weeks after implantation (N=6, mean ± SD). *: $P<0.05$.

Abbreviations: RCP, recombinant human collagen-peptide based scaffold; TCP, tricalcium phosphate.